Electronical Supporting Information (ESI): Spatial mapping and scaling of the shear-induced transformation from bicontinuous microemulsions towards lamellar structures by coupling microfluidics and SANS†

Julian Fischer,[a] Lionel Porcar,[b] João T. Cabral,[c] and Thomas Sottmann[a*]

S1 Details on scattering analysis

Azimuthal analysis

To quantify the structural flow response of bicontinuous D_2O/*n*-octane/$C_{10}E_4$ microemulsions with respect to the degree of anisotropy, the scattering intensity around the maximum of the isotropic pattern was analyzed azimuthally as described in Sec. III B of the main article. Due to the shift of the scattering maximum with membrane volume fraction, the respective q-ranges were adjusted accordingly to 1.6×10^{-2} to 3.1×10^{-2} Å^{-1} at $\phi_m = 0.137$, 1.3×10^{-2} to 2.9×10^{-2} Å^{-1} at $\phi_m = 0.125$ and 1.1×10^{-2} to 2.7×10^{-2} Å^{-1} at $\phi_m = 0.110$. The resulting $I(\chi)$-curves and their analysis are shown in Fig. 5b of the main article.

Radial analysis

More information on length scale and other membrane properties of the flow-induced structure are obtained by averaging the 2D scattering patterns radially as described in Sec. II C2 of the main article. Analyzing the resulting $I(q)$-curves with respect to the bicontinuous nature of the studied D_2O/*n*-octane/$C_{10}E_4$ microemulsion at rest, which has been demonstrated by means of freeze fracture transmission electron microscopy[1], we used the Teubner-Strey model[2]:

$$I(q) = \frac{1}{c_2 q^4 + c_1 q^2 + a_2} \tag{S1}$$

to describe our data. Here, a_2, c_1 and c_2 are the coefficients of the order parameter expansion of the free energy density f[3]. This description of the scattering intensity, shown in Eq. (S1), is obtained by Fourier transformation of the spatial correlation function:

$$\gamma(r) = \frac{\sin(kr)}{kr} \times \exp\left(\frac{-r}{\xi_{TS}}\right) \tag{S2}$$

where $k = 2\pi/d_{TS}$. Note that the random wave description of Marčelja et al.[4,5] formally gives the same scattering intensity function as Eq. (S1), while the clipped random wave model of Chen et al.[6,7] uses an additional third length scale introduced by a higher order term in the spectral density function.

Nevertheless, Eq. (S2) combines the two well-known properties of symmetric bicontinuous microemulsions. First, water and oil form alternating domains of size $\xi = d_{TS}/2$, which are separated by an amphiphilic film. Second, there is no long-range order, characterized by the correlation length ξ_{TS}. In terms of a_2, c_1 and c_2, these two structural length scales are given by:

$$d_{TS} = 2\pi\left[\frac{1}{2}\left(\frac{a_2}{c_2}\right)^{1/2} - \frac{c_1}{4c_2}\right]^{-1/2} \tag{S3}$$

and

$$\xi_{TS} = \left[\frac{1}{2}\left(\frac{a_2}{c_2}\right)^{1/2} + \frac{c_1}{4c_2}\right]^{-1/2} \tag{S4}$$

[a] *Instiute of Physical Chemistry, University of Stuttgart, Pfaffenwaldring 55, 70569 Stuttgart, Germany.*
[b] *Institut Laue-Langevin, 71 Avenue des Martyrs, CS 20156, 38042 Grenoble CEDEX 9, France.*
[c] *Department of Chemical Engineering, Imperial College London, London SW7 2AZ, United Kingdom.*
[*] *Corresponding Author. Tel: +49 711 685 64494; E-mail: thomas.sottmann@ipc.uni-stuttgart.de*

† This document presents supporting information to the article "Spatial mapping and scaling of the shear-induced bicontinuous-to-lamellar transition in microemulsions by coupling microfluidics and SANS". See DOI: 10.1039/cXsm00000x/

S2 Comparative scattering data measured in quartz cells

For the measurements of the bicontinuous D_2O/*n*-octane/$C_{10}E_4$ microemulsions in quartz cells, multiple collimation/detector distances were utilized, 2.8 m/2.0 m, 8.0 m/8.0 m and 17.6 m/17.6 m for the sample with a membrane volume fraction of $\phi_m = 0.137$ as well as 5.6 m/5.6 m and 17.6 m/17.6 m for the samples with $\phi_m = 0.110$ and 0.125. Note that for the latter two samples an additional side detector was used, extending the q range to higher values. Thus, the scattering intensities were detected over q-ranges from 2.6×10^{-3} to 4.3×10^{-1} Å^{-1} ($\phi_m = 0.137$) and 3.9×10^{-3} to 6.4×10^{-1} Å^{-1} ($\phi_m = 0.110$ and 0.125), respectively. Fig. S1 shows select 2D scattering patterns of all three samples as well as the $I(q)$-curves resulting from their radial analysis.

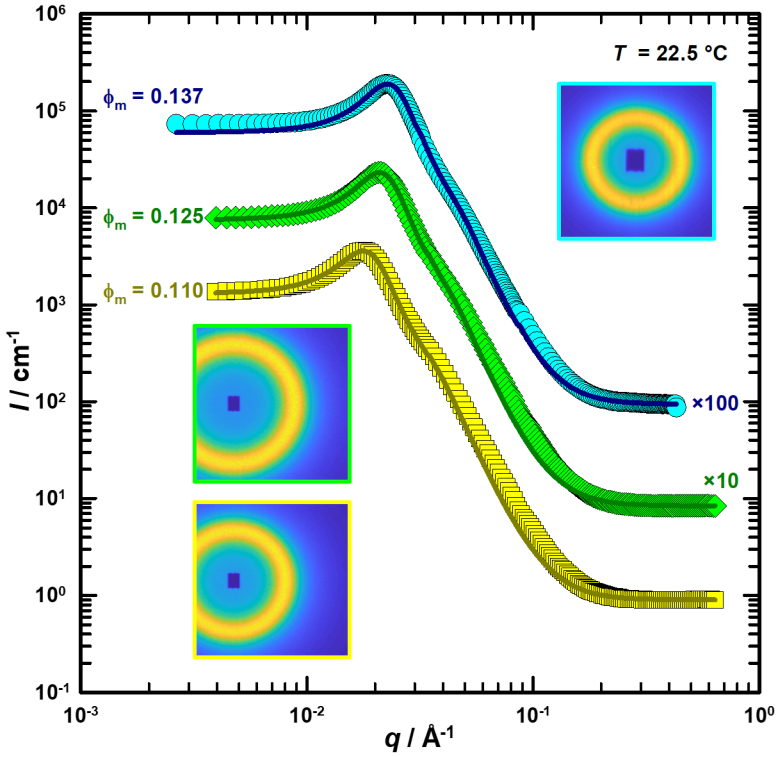

Fig. S1 2D scattering patterns measured in quartz cells and resulting intensity profiles as a function of the scattering momentum transfer q of bicontinuous D_2O/*n*-decane/$C_{10}E_4$ microemulsions at membrane volume fractions of $\phi_m = 0.110$ (yellow squares), 0.125 (green diamonds) and 0.137 (cyan circles). The $I(q)$-curves are analyzed with the model of Teubner and Strey[2] (Eq. (S1)) taking into account multiple scattering[8–10]. The corresponding results are listed in Table S1.

The $I(q)$-curves are analyzed with the model of Teubner and Strey[2] (Eq. (S1)) taking into account multiple scattering[8–10] (∼1 mm sample thickness). The corresponding results are listed in Table S1 and compared to the microfluidic results from the main article. Both agree almost quantitatively and slight deviations can be readily justified with the assumption of a pure single scattering contribution for the microfluidic measurements due to their small sample thickness of ∼300 μm.

Table S1 Periodicity d_{TS} and correlation length ξ_{TS} obtained from the analysis of SANS measurements performed in quartz cells and a microfluidic device on D_2O/*n*-octane/$C_{10}E_4$ microemulsions with different membrane volume fractions ϕ_m at $T = 22.5\,°C$. The corresponding scattering curves are shown in Fig. S1 (quartz cells) and Fig. 5c of the main article (microfluidic device).

ϕ_m	sample environment	d_{TS} / Å	ξ_{TS} / Å
0.137	quartz cell	267	179
	microfluidic device	260	174
0.125	quartz cell	289	190
	microfluidic device	285	181
0.110	quartz cell	339	211
	microfluidic device	332	191

S3 Additional spatial mapping data

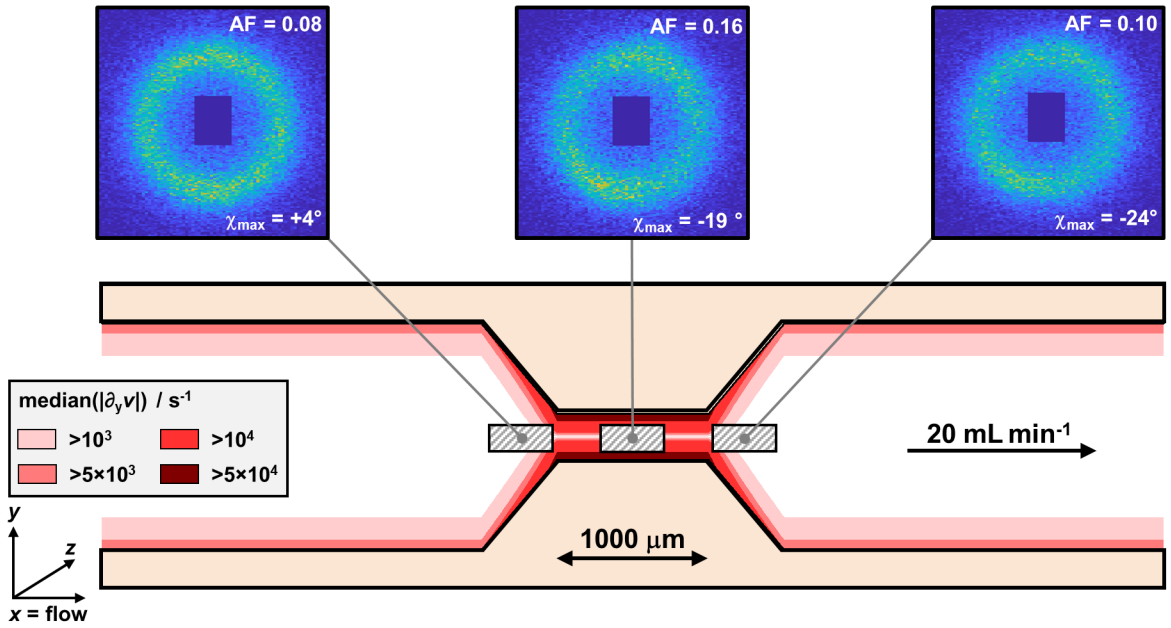

Fig. S2 2D scattering patterns of a bicontinuous D_2O/*n*-octane/$C_{10}E_4$ microemulsion ($\phi_m = 0.137$) flowing along a microfluidic constriction. Spatial mapping of the alignment factor AF and the orientation angle χ_{max} confirms the promotion of the shear-induced bicontinuous-to-lamellar transition due to the compression before the constriction as already reported in the main article. The measurements additionally suggest the partial conservation of the induced structure in the extensional flow after the constriction.

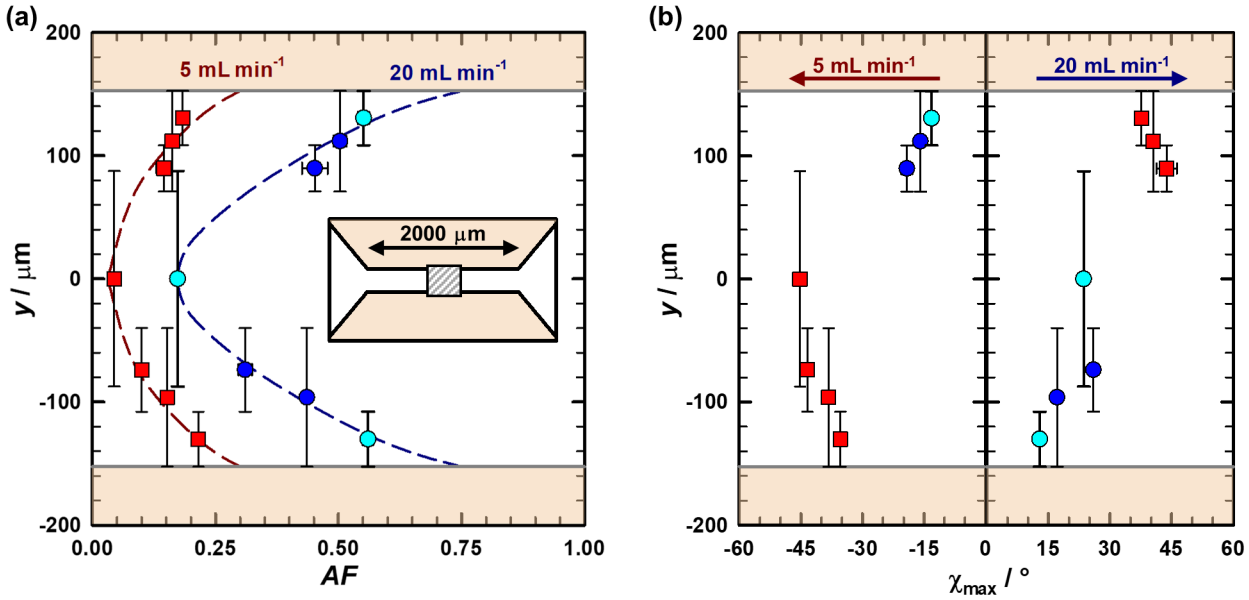

Fig. S3 Alignment factor AF (a) and orientation angle χ_{max} (b) of a bicontinuous D_2O/*n*-octane/$C_{10}E_4$ microemulsion ($\phi_m = 0.137$) under flow as a function of the vertical position y inside the microfluidic constriction. The results are measured at flow rates of $5\,\mathrm{mL\,min^{-1}}$ (red squares) and $20\,\mathrm{mL\,min^{-1}}$ (blue circles), including those already shown in the main article (cyan circles). Both AF and χ_{max} invert their behavior at the channel center ($y = 0\,\mu\mathrm{m}$), with χ_{max} also changing its sign. The orientation angle also depends on the different flow directions at 5 (right-to-left) and $20\,\mathrm{mL\,min^{-1}}$ (left-to-right). With exception of the results at $y = 0\,\mu\mathrm{m}$, all data are also shown in the $|\chi_{max}|$ vs. AF plot of Fig. 4 in the main article.

S4 Raw data of the scaling study

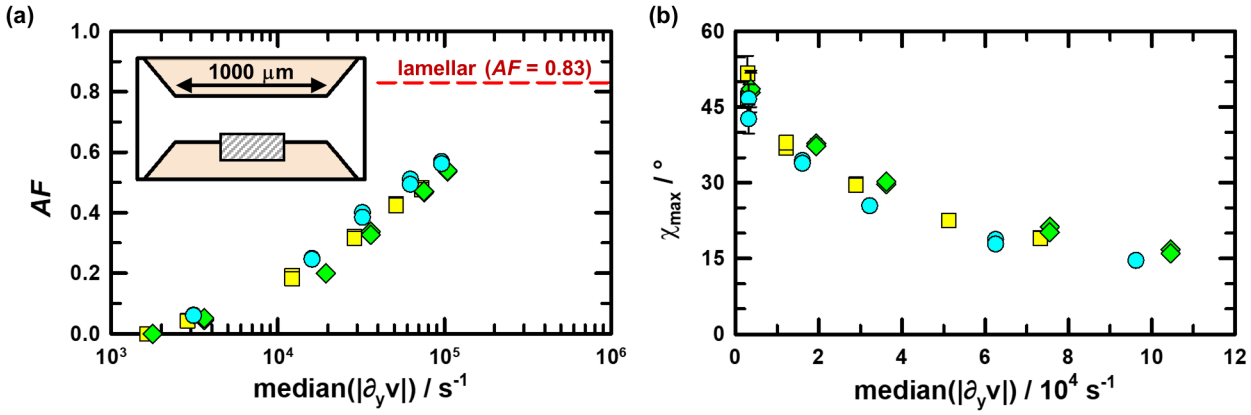

Fig. S4 Alignment factor AF (a) and orientation angle χ_{max} (b) of bicontinuous D_2O/*n*-octane/$C_{10}E_4$ microemulsions flowing at the wall of a microfluidic constriction as a function of the median $|\partial_y v|$. The microemulsions are located at membrane volume fractions of $\phi_m = 0.110$ (yellow squares), 0.125 (green diamonds) and 0.137 (cyan circles). These results are also shown in Fig. 6a and b of the main article with a scaled shear axis.

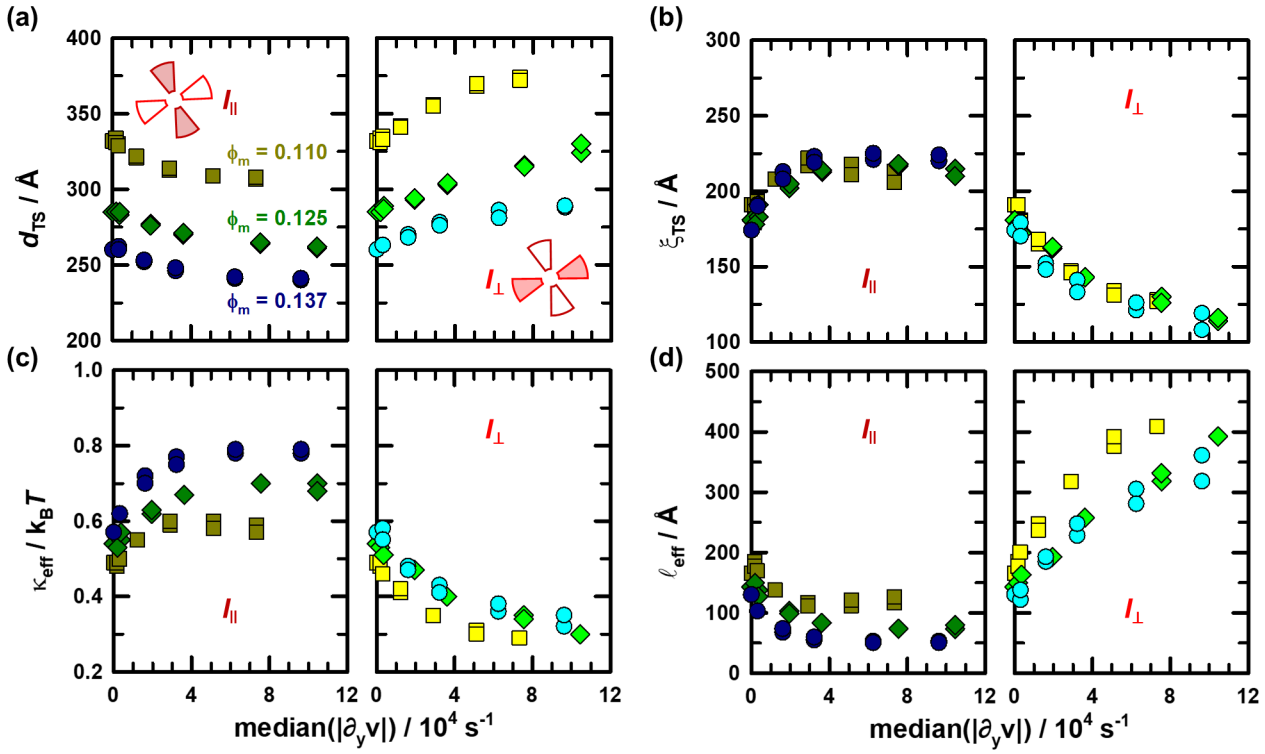

Fig. S5 Periodicity d_{TS} (a), correlation length ξ_{TS} (b), effective bending rigidity κ_{eff} (c) and effective fluctuation length scale ℓ_{eff} (d) of bicontinuous D_2O/*n*-octane/$C_{10}E_4$ microemulsions flowing at the wall of a microfluidic constriction as a function of the median $|\partial_y v|$. The microemulsions are located at membrane volume fractions of $\phi_m = 0.110$ (yellow squares), 0.125 (green diamonds) and 0.137 (cyan circles). The left side of each graph shows the respective parameter along the main orientation of the structure ($\parallel$), while the right side shows the perpendicular orientation ($\perp$). The ℓ_{eff} results are also shown in Fig. 6b of the main article with a scaled shear axis.

S5 Scaled data for length scales d_{TS} and ξ_{TS}

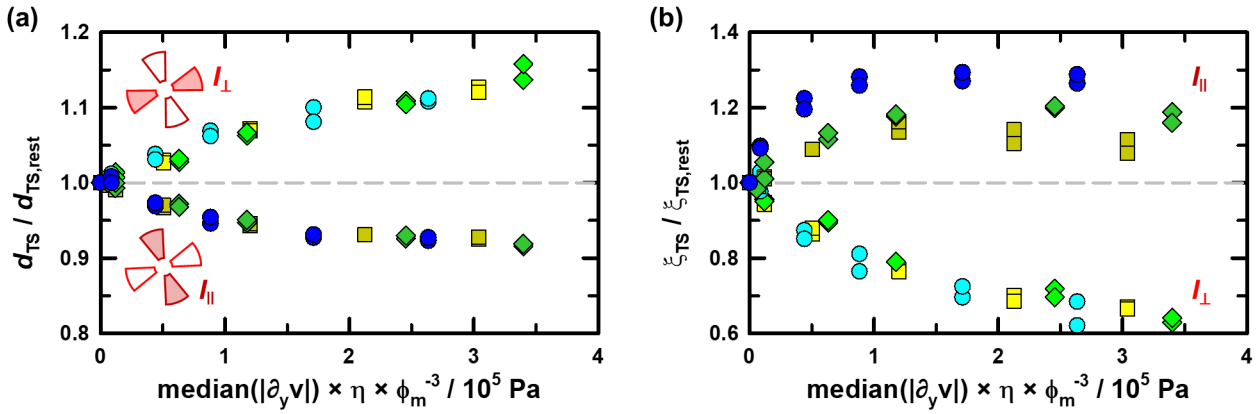

Fig. S6 Normalized periodicity $d_{TS}/d_{TS,rest}$ and correlation length $\xi_{TS}/\xi_{TS,rest}$ as a function of median $(|\partial_y v|) \times \eta \times \phi_m^{-3}$. Both length scales are normalized by their respective values at rest and are plotted against a shear axis which is scaled according to the theory of Cates and Milner[11] (Eq. (3) of the main article). While the scaling of ξ_{TS} shows the same deviation as discussed in the main article, d_{TS} agrees almost quantitatively with the applied scaling relation. We argue that ξ_{TS} strongly depends on the topology of the microemulsion and thus is more influenced by the highest membrane volume fraction than the solely geometric distance between surfactant monolayers given by $\xi = d_{TS}/2$.

S6 Error Analysis

The standard errors of the alignment factor AF and tilt angle χ_{max} result from fitting the azimuthal scattering data with the elliptical equation, as described in Sec. III B of the main article. They lie in the range of

$$0.005 < \Delta AF < 0.012$$

and

$$0.4^\circ < \Delta\chi_{max} < 4^\circ$$

The relative errors of the periodicity d_{TS} and correlation length ξ_{TS} were estimated with

$$\frac{\Delta d_{TS}}{d_{TS}} = 0.01$$

and

$$\frac{\Delta \xi_{TS}}{\xi_{TS}} = 0.02$$

The errors of the effective bending rigidity κ_{eff}, the bare bending rigidity κ_0 and the effective fluctuation length scale ℓ_{eff} were calculated accordingly:

$$\frac{\Delta \kappa_{eff}}{\kappa_{eff}} = \frac{\Delta d_{TS}}{d_{TS}} + \frac{\Delta \xi_{TS}}{\xi_{TS}} = 0.03$$

$$\Delta\kappa_0 = 0.02\ k_B T$$

$$\frac{\Delta \ell_{eff}}{\ell_{eff}} = \frac{4\pi}{\alpha} \times \left(\frac{\Delta\kappa_0}{k_B T} + \frac{\Delta\kappa_{eff}}{k_B T} \right)$$

Notes and references

1 T. Sottmann, *Mikroemulsionen: Eigenschaften von internen Grenzflächen*, Cuvillier, Göttingen, 1st edn., 1998.

2 M. Teubner and R. Strey, *The Journal of Chemical Physics*, 1987, **87**, 3195–3200.

3 L. D. Landau and E. M. Lifschitz, *Statistische Physik Teil 1*, Akademie-Verlag Berlin, Berlin, 8th edn., 1979, vol. 5.

4 P. Pieruschka and S. Marčelja, *Journal de Physique II*, 1992, **2**, 235–247.

5 L. Arleth, S. Marčelja and T. Zemb, *The Journal of Chemical Physics*, 2001, **115**, 3923–3936.

6 D. Choy and S. H. Chen, *Physical Review E*, 2000, **61**, 4148–4155.

7 S. M. Choi, S. H. Chen, T. Sottmann and R. Strey, *The Journal of Chemical Physics*, 2002, **304**, 85–92.

8 J. Schelten and W. Schmatz, *Journal of applied crystallography*, 1980, **13**, 385–390.

9 J. A. Silas and E. W. Kaler, *Journal of colloid and interface science*, 2003, **257**, 291–298.

10 G. V. Jensen and J. G. Barker, *Journal of applied crystallography*, 2018, **51**, 1455–1466.

11 M. E. Cates and S. T. Milner, *Physical review letters*, 1989, **62**, 1856–1859.